



HAL
open science

p16INK4a deficiency promotes IL-4-induced polarization and inhibits proinflammatory signaling in macrophages.

Céline Cudejko, Kristiaan Wouters, Lucía Fuentes, Sarah Anissa Hannou, Charlotte Paquet, Kadiombo Bantubungi, Emmanuel Bouchaert, Jonathan Vanhoutte, Sébastien Fleury, Patrick Remy, et al.

► **To cite this version:**

Céline Cudejko, Kristiaan Wouters, Lucía Fuentes, Sarah Anissa Hannou, Charlotte Paquet, et al.. p16INK4a deficiency promotes IL-4-induced polarization and inhibits proinflammatory signaling in macrophages.: p16INK4a function in macrophages. *Blood*, 2011, 118 (9), pp.2556-66. 10.1182/blood-2010-10-313106 . inserm-00605106

HAL Id: inserm-00605106

<https://inserm.hal.science/inserm-00605106>

Submitted on 30 Jun 2011

HAL is a multi-disciplinary open access archive for the deposit and dissemination of scientific research documents, whether they are published or not. The documents may come from teaching and research institutions in France or abroad, or from public or private research centers.

L'archive ouverte pluridisciplinaire **HAL**, est destinée au dépôt et à la diffusion de documents scientifiques de niveau recherche, publiés ou non, émanant des établissements d'enseignement et de recherche français ou étrangers, des laboratoires publics ou privés.

p16^{INK4a}-deficiency promotes IL-4-induced polarization and inhibits pro-inflammatory signaling in macrophages

Céline CUDEJKO^{1,2,3,4,†}, Kristiaan WOUTERS^{1,2,3,4,†}, Lucía FUENTES^{1,2,3,4}, Sarah Anissa HANNOU^{1,2,3,4}, Charlotte PAQUET^{1,2,3,4}, Kadiombo BANTUBUNGI^{1,2,3,4}, Emmanuel BOUCHAERT^{1,2,3,4}, Jonathan VANHOUTTE^{1,2,3,4}, Sébastien FLEURY^{1,2,3,4}, Patrick REMY^{4,5}, Anne TAILLEUX^{1,2,3,4}, Giulia CHINETTI^{1,2,3,4}, David DOMBROWICZ^{1,2,3,4}, Bart STAELS^{1,2,3,4,*} and Réjane PAUMELLE^{1,2,3,4}.

1 Univ. Lille Nord de France, F-59000, Lille, France

2 Inserm, U1011, F-59000, Lille, France

3 UDSL, F-59000, Lille, France

4 Institut Pasteur de Lille, F-59019, Lille, France

5 Service de Production des antigènes, Institut Pasteur de Lille, F-59019, Lille, France

Short title: p16^{INK4a} function in macrophages

* Corresponding author: Bart Staels, Inserm UR 1011, Institut Pasteur de Lille, 1 rue du Professeur Calmette, BP 245, Lille 59019, France, Tel: +33 3 20 87 73 88, Fax: +33 3 20 87 73 60, E-mail: bart.staels@pasteur-lille.fr

† These authors contributed equally to this work.

Word count: 4900

Abstract count: 196

Figure count: 7 (and 10 Supplemental Figures)

Table count: 2 (and 4 Supplemental Tables)

Reference count: 50

ABSTRACT

The *CDKN2A* locus, which contains the tumor suppressor gene p16^{INK4a}, is associated with an increased risk of age-related inflammatory diseases, such as cardiovascular disease and type 2 diabetes, in which macrophages play a crucial role. Monocytes can polarize towards classically (CAM ϕ) or alternatively (AAM ϕ) activated macrophages. However, the molecular mechanisms underlying the acquisition of these phenotypes are not well defined.

Here, we show that p16^{INK4a}-deficiency (p16^{-/-}) modulates the macrophage phenotype. Transcriptome analysis revealed that p16^{-/-} bone marrow-derived macrophages (BMDM) exhibit a phenotype resembling interleukin (IL)-4-induced macrophage polarization. In line with this observation, p16^{-/-} BMDM displayed a decreased response to classically polarizing IFN γ and LPS and an increased sensitivity to alternative polarization by IL-4. Furthermore, mice transplanted with p16^{-/-} bone marrow displayed higher hepatic AAM ϕ marker expression levels upon *Schistosoma mansoni* infection, an *in vivo* model of AAM ϕ phenotype-skewing. Surprisingly, p16^{-/-} BMDM did not display increased IL-4-induced STAT6 signaling, but decreased IFN γ -induced STAT1 and LPS-induced IKK α,β phosphorylation. This decrease correlated with decreased JAK2 phosphorylation and with higher levels of inhibitory acetylation of STAT1 and IKK α,β . These findings identify p16^{INK4a} as a modulator of macrophage activation and polarization via the JAK2-STAT1 pathway with possible roles in inflammatory diseases.

INTRODUCTION

The tumor suppressor p16^{INK4a} is encoded by the *CDKN2A* locus on the human chromosome 9p21 and on the murine chromosome 4. p16^{INK4a} belongs to the INK4 family of cyclin-dependent kinase (CDK) inhibitors, also including p15^{INK4b}, p18^{INK4c}, and p19^{INK4d} 1-5. p16^{INK4a} inhibits cell cycle progression by preventing cyclin D-CDK 4/6 complex formation. As a consequence, pRb hyperphosphorylation and its association with E2F, which induces transcription of S phase genes, are inhibited. p16^{INK4a} inactivation by deletion, point mutation or promoter methylation, occurs frequently in most tumors ⁶.

Besides its role in cancer as an inhibitor of cell cycle progression, p16^{INK4a} plays a crucial role in senescence and aging ^{7, 8}. Indeed, expression of p16^{INK4a} increases with age in various tissues from several species ^{9, -11}. A genome-wide association study has shown association of the *CDKN2A* locus with an increased risk of the age-related frailty syndrome ¹². Additionally, increased p16^{INK4a} expression causes the age-dependent decline in proliferation of self-renewing cellular compartments such as haematopoietic stem cells ¹³, which give rise to immune cells.

Although the role of p16^{INK4a} in mature immune cells has not yet been investigated, a number of studies has shown that the *CDKN2A* locus is associated with an increased risk for coronary heart disease ¹⁴, atherosclerosis ¹⁵, and type 2 diabetes (T2D) ¹⁶. In these pathologies, immune cells, such as macrophages, play a crucial role. Besides their pleiotropic immune functions, macrophages also play a role in the development and homeostasis of several tissues, such as adipose tissue ¹⁷ and liver ¹⁸. Depending upon the cytokine environment, macrophages differentiate into distinct subclasses with specific characteristics. Classically activated macrophages (CAM ϕ) differentiate in presence of Th1 cytokines, such as interferon gamma (IFN γ), or in presence of bacterial products such as lipopolysaccharide (LPS). CAM ϕ trigger pro-inflammatory responses required to kill intracellular pathogens ¹⁹. Alternatively activated macrophages (AAM ϕ), induced by Th2 cytokines such as interleukin (IL)-4 and IL-13, are associated with Th2-type immune

responses as seen in helminth parasite infections [1]. During inflammation, AAM ϕ play a key role in protecting the organism against tissue damage [2]. However, little is known about the mechanisms underlying the acquisition of the AAM ϕ phenotype.

In the present study, we investigated whether p16^{INK4a}-deficiency influences macrophage activation *in vitro*, using bone marrow-derived macrophages (BMDM), and *in vivo* by infection with the parasite *Schistosoma mansoni*. BMDM from p16^{INK4a}-deficient (p16^{-/-}) mice exhibit a phenotype resembling IL-4-induced macrophage polarization and an enhanced response to the Th2 cytokine IL-4 compared to BMDM from wild type (p16^{+/+}) mice. By contrast, their response to Th1 stimuli is diminished. Moreover, *Schistosoma mansoni* infection of mice transplanted with p16^{-/-} bone marrow resulted in an increased hepatic AAM ϕ signature *in vivo*. Finally, we show that p16^{INK4a}-deficiency does not influence the IL-4-induced STAT6 pathway. By contrast, the lower response to classical activation stimuli likely occurs through an inhibition of the phosphorylation of both STAT1 and IKK α,β , which correlated with decreased JAK2 phosphorylation and increased acetylation of STAT1 and IKK α,β ,

METHODS

Mice. C57BL/6J p16^{INK4a}-deficient and littermate control mice on a C57Bl6 background (>97%) were kindly provided by P. Krimpenfort. p16^{-/-} mice showed neither abnormalities in biochemical parameters nor spontaneous tumor development at the studied age. Flow cytometry analysis of splenic T- and B-cells or macrophages showed no differences between p16^{-/-} and p16^{+/+} mice (data not shown). All protocols were conducted with the approval of the Pasteur Institute ethical review board, Lille, France.

Bone marrow chimeras. 8 week-old C57BL/6J mice were lethally irradiated (8 Gy) and injected in the tail vein the next day with 10x10⁶ bone marrow cells isolated from p16^{-/-} or p16^{+/+} donor mice. Mice were supplied with autoclaved acidified water (pH=2) supplemented with neomycin 100 mg/L (Cat.N1142, Sigma-Aldrich), polymyxin B sulphate 60000 U/L (Cat.21850029, Invitrogen) 1 week before and 4 weeks after transplantation. Mice were studied 6 weeks post-transplantation to allow repopulation by the donor bone marrow. To ensure that donor bone marrow replaced the resident blood cell population, DNA was extracted from whole blood with an Illustra blood kit (GE Healthcare). PCR was performed with forward 5'-GCA-GTG-TTG-CAG-TTT-GAA-CCC-3' and reverse 5'-TGT-GGC-AAC-TGA-TTC-AGT-TTG-3' primer sets yielding products of different lengths, which were separated on a 1.5% agarose gel and quantified with the Gel Doc XR system (Bio-Rad). Over 95% of host blood cells were from donor origin.

Primary cell isolation and culture. LPS-elicited neutrophils from air pouches were isolated as described²¹. Splenic CD4⁺ T-cells and CD43⁻ B-cells were isolated from female mice respectively using Dynal (Invitrogen), biotin-conjugated anti-CD43 (Becton Dickinson) and streptavidin conjugated to magnetic beads (Miltenyi Biotech) according to manufacturer's instructions. Bone marrow-derived dendritic cells were prepared as described²². BMDM were obtained from femoral and tibial bone marrow suspensions, plated at 10x10⁶ cells in 10 cm plates and differentiated in BMDM medium (RPMI 1640 containing Hepes 25 mM

supplemented with 10% low endotoxin fetal bovine serum, 15% L929-conditioned medium, 2 mM L-glutamine, 1 mM gentamycin). Stimulations and microarray analysis were carried out at day 8. IL-4 (15 ng/mL) and IFN γ (2.5 ng/mL and 10 ng/mL) were obtained from Peprotech. LPS (100 ng/mL) from *E. coli* serotype 0111B4 was from Sigma-Aldrich. CINK4 (#219492) was obtained from Merck. For indirect co-culture experiments, conditioned medium of alternatively differentiated p16^{+/+} and p16^{-/-} macrophages was added to cultures of BMDM 24h before LPS (100 ng/mL) stimulation. After 4h, CAM ϕ were washed and cultured for 24h in fresh medium. The resulting media were assayed for cytokine secretion by ELISA.

Flow cytometry. During *in vitro* differentiation, asynchronously growing cultures of BMDM were gently scraped every two days with PBS 1X/EDTA 10 mM/2% trypsin, washed with PBS and collected by centrifugation (5 min, 900 rpm). For protein analysis, non-specific staining was avoided by incubating cells with purified rat anti-mouse CD16/CD32 (Cat.553141, BD Pharmingen) for 20 min at 4°C and labeled with anti-mouse F4/80-FITC (Cat.RM2901, Caltag Laboratories) for 30 min at 4°C. Cells were analyzed using a Coulter EPICS XL4-MCL[®] Flow cytometer (BeckmanCoulter) and Expo32[®] software (Applied Cytometry Systems). For cell sorting, cells were incubated with anti-mouse F4/80-FITC antibodies (11-4801, eBioscience) and Rat IgG2a K isotype (11-4321, eBioscience) and sorted on an EPICS-ALTRA cell sorter (Beckman Coulter). For FACS-based cell cycle analysis, cells were fixed with 70% ethanol for 1h at -20°C and labeled with 50 μ g/mL propidium iodide containing 50 μ g/mL RNase A for 30 min at room temperature. The percentage of cell cycle distribution was obtained using the Multicycle[®] software (Phoenix Flow systems).

Microarray studies. Mouse genome MOE 430 2.0 gene chips (Affymetrix[®]) were used in triplicate for each condition. Sample preparation, hybridization and scanning were performed according the One-cycle protocol (Affymetrix[®]). Only genes significantly regulated ($p < 0.05$)

were analyzed further with Genomatix Bibliosphere[®]. Microarray data have been deposited to <http://www.ebi.ac.uk/arrayexpress>.

RNA extraction and analysis. Total RNA was obtained from BMDM using EXTRACT-ALL[®], DNase-I treated, and cDNA was generated using cDNA reverse transcription kit (AB Applied Biosystems). Real-time QPCR detection was conducted on a Stratagene Mx3005P[®] (Agilent technologies) using Brilliant II SYBR Green reagent[®] (Agilent Technologies) and specific primers (Table S1). mRNA levels were normalized to 36B4 mRNA and fold induction was calculated using the $2^{-\Delta\Delta Ct}$ method.

Cytokine production measurement. IL-6, TNF, IL-1Rn, IL-4, IL-10 and IFN γ levels in culture supernatants were measured with ELISA kits according to the manufacturer's instructions (R&D systems). Plasma IgE from infected animals was determined by ELISA using purified rat anti-mouse IgE (Cat.553416, BD Pharmingen) as a capture antibody, and biotin rat anti-mouse IgE as a detection antibody (Cat.553414, BD Pharmingen). Standards were prepared using purified mouse IgE κ isotype control (Cat.557079, BD Pharmingen).

Protein extraction and Western blotting. BMDM lysates were prepared using Cell Lysis Buffer (#9803, Cell Signaling Technology) supplemented with 1 mM PMSF. Lysates were resolved in 16% or 10% SDS-PAGE and analyzed by western-blot. Anti-p16 (sc-1207), -actin (sc-1616) and -p38 (sc-535) antibodies were purchased from Santa Cruz Biotechnology. Anti-phospho-STAT6 and -STAT6 (#9361 and 9362), anti-phospho-STAT1 and -STAT1 (#9171 and 9172), anti-phospho-p38 (#9211), anti-phospho-IKK α,β (#2681), anti-I κ B α (#9242) and anti-phospho-JAK2 and -JAK2 (#3771 and 3230) antibodies were purchased from Cell Signaling Technology. Hybridizations were done 1:1000 in 5% BSA, 1X TBS, 0.1% Tween-20 overnight at 4°C. Anti-rabbit IgG Peroxidase conjugate secondary antibody 1:10000 (Cat.A-0545, Sigma-Aldrich) was added for 1h at room temperature. Signals were

visualized using the enhanced chemiluminescence Western blot detection kit (Amersham ECL plus Western blotting Detection System; GE Healthcare). Membranes were stripped with Reblot Plus Strong Antibody Stripping Solution[®] (Cat.2504, Millipore) and re-blotted with the indicated antibodies.

Immunoprecipitation (IP) assay. 500 µg of BMDM lysates were prepared using lysis buffer supplemented with trichostatin A 1 µM (Cat.T8552, Sigma-Aldrich). Lysates were mixed with 100 µL of Protein G/Protein A Agarose (Millipore) and rotated for 1h at 4°C. After centrifugation for 2 min at 3000 rpm, anti-acetyl-Lysine antibody 1:100 (ab21623, Abcam) was added. Samples were rotated overnight at 4°C. The Protein G/Protein A Agarose mix (100 µL) was added to the samples and incubated for 1h at 4°C. The beads were washed 3x and the pellets dissolved in 40 µL of Laemmli 2X buffer. Proteins were analyzed by western blotting as previously described.

S. mansoni infection. Chimeric mice were anesthetized and percutaneously infected with 40 *S. mansoni* cercariae and sacrificed 9 weeks later. The liver was perfused and adult worms were recovered and quantified. A piece of liver was weighed and dissolved in a KOH solution (5%, 37°C during 16h) and eggs were counted. Organs were snap frozen or fixed in paraformaldehyde for further analysis. Resin-embedded livers were cut at 5 µm and Mallory's Trichrome staining was performed to determine granuloma size and hepatic collagen. Immunostaining was performed using antibodies directed to Moma-2 (sc59332, Santa Cruz), Arginase1 (Arg-I) (ab60176-100), Fizz1 (ab39626-50) and Ym1 (ab93034) from Abcam. May Grunwald Giemsa staining was performed and eosinophils were counted per granuloma area. Granulomas were isolated using an Arcturus Laser capture microdissection system from 14 µm sections of snap frozen liver samples. For *ex vivo* restimulation, spleens were homogenized, filtered (70 µm) and erythrocytes were lysed. Cells were cultured in RPMI 1640 (Gibco) supplemented with 10% low endotoxin fetal bovine serum and 1 mM gentamycin. 5×10^5 cells were stimulated with 10 µg/ml soluble egg antigen (SEA) or anti-

CD3 (#555274; BD Pharmingen) antibodies during 4 days after which medium was collected for cytokine determination by ELISA.

Statistical analysis.

Groups were compared using 2-tailed non-paired *t*-tests using GraphPad Prism® software. *In vitro* data are expressed as means ± SD and *in vivo* data are expressed as means ± SEM.

RESULTS

p16^{INK4a} expression increases during macrophage maturation, but p16^{INK4a}-deficiency does not modulate macrophage cell cycle progression.

In order to assess whether and in which mature immune cell types p16^{INK4a} is expressed, p16^{INK4a} mRNA was measured in dendritic cells (DC), bone marrow-derived macrophages (BMDM) and neutrophils, all of myeloid origin, and in B- and T-lymphocytes. p16^{INK4a} was highly expressed in BMDM and DC, while its expression was markedly lower in neutrophils and virtually absent in lymphocytes (Figure 1A). Since the *CDKN2A* locus has been associated to diseases with inflammatory components in which macrophages play a central role, we focused on the role of p16^{INK4a} in these cells. BMDM displayed a gradual increase in p16^{INK4a} mRNA expression during *in vitro* differentiation (Figure 1B). Cell sorting analysis showed that p16^{INK4a} mRNA expression increased specifically in F4/80-positive cells (macrophages) (Figure S1). Together, these data show that increased expression occurs in a higher number of macrophages which also express higher p16^{INK4a} levels. In line, p16^{INK4a} protein was expressed in differentiated macrophages (Figure 1C). Absence of p16^{INK4a} (Figure 1C) did not influence macrophage maturation, since it affected neither mRNA (Figure 1D) nor protein (Figure 1E) expression of the macrophage surface marker F4/80 during differentiation. Interestingly, absence of p16^{INK4a} did not affect cell cycle progression at any time point of *in vitro* macrophage differentiation (Figure 1F). Expression analysis of the INK4 family members p15^{INK4b}, p18^{INK4c}, p19^{INK4d} and p19^{ARF}, another product of the *INK4A/ARF* locus which inhibits the p53 pathway, as well as the KIP/CIP family members p21^{WAF1} and p27^{KIP1} revealed increased expression of p15^{INK4b} in p16^{INK4a}-deficient (p16^{-/-}) BMDM (Fig. S2). Together with the observation that expression of Cyclin D, a direct E2F target gene, is similar in both genotypes (Figure S3), these data suggest that the induction of p15^{INK4b} may compensate for p16^{INK4a}-deficiency in the control of the cell cycle. These data indicate that p16^{INK4a} expression increases during macrophage differentiation and that p16^{INK4a}-deficiency influences neither maturation nor the cell cycle in BMDM.

Macrophage p16^{INK4a}-deficiency leads to a phenotype resembling IL-4-induced macrophage polarization.

Microarray analysis of p16^{-/-} BMDM revealed that the expression of a large number of inflammatory genes was significantly lower compared to wild type (p16^{+/+}) BMDM under basal conditions (Figure 2A). Several of these genes are typically associated with a CAM ϕ phenotype²³⁻²⁷. By contrast, a number of AAM ϕ -associated genes, linked to IL-4-induced STAT6 activation²³⁻²⁷, were significantly higher expressed in p16^{-/-} BMDM (Figure 2B). However, the AAM ϕ markers Ym1/2 and Fizz1 were not spontaneously induced by p16^{INK4a}-deficiency. The differential expression of a number of these genes was confirmed by QPCR (Table S2).

To further characterize this IL-4-like phenotype of p16^{-/-} BMDM, the gene signature of these cells was compared with the gene signature of p16^{+/+} BMDM polarized *in vitro* by addition of IL-4 from day 0 of differentiation, generating p16^{+/+} AAM ϕ ²⁸. Compared to p16^{+/+} BMDM, 14311 probesets were differentially expressed in p16^{+/+} AAM ϕ (Figure 2C, green dots), whereas 7605 probesets were regulated in p16^{-/-} BMDM (Figure 2C, red dots), of which the majority (78%) was also differentially expressed in p16^{+/+} AAM ϕ (Figure 2C, blue dots). In addition, a strong correlation ($p < 0.0001$; Pearson $R = 0.7$; $R^2 = 0.5$) was found between the two experimental conditions (Figure 2C), as also illustrated by a heat map representation of a selection of AAM ϕ and CAM ϕ marker genes (Figure 2D and Table S3).

Since p16^{-/-} BMDM displayed lower expression levels of inflammatory genes (Figure 2A, D), the secretion of inflammatory cytokines produced in p16^{-/-} BMDM compared to p16^{+/+} BMDM was measured. Under basal conditions, secretion of the pro-inflammatory cytokines IL-6 and TNF was lower (Figure 3A, B) in p16^{-/-} BMDM. By contrast, secretion of anti-inflammatory IL-1Rn was, albeit modestly, higher (Figure 3C). These observations are in line with the microarray data and suggest that p16^{-/-} BMDM are functionally different from their wild type counterparts.

Next, we compared the response of p16^{-/-} vs. p16^{+/+} BMDM to polarization into AAM ϕ induced by IL-4 added at the start (day 0) of differentiation. Induction of the AAM ϕ marker genes Arg-I (Figure 3D) and Ym1/2 (Figure 3E) was higher in p16^{-/-} AAM ϕ . However, induction of Mgl2 (Figure 3F) was not different in these cells, suggesting that the IL-4-responsiveness of certain, but not all, genes is dependent on p16^{INK4a}. This heterogeneity in regulation of AAM ϕ marker genes in IL-4-polarized p16^{-/-} AAM ϕ confirms the microarray results (Figure 2D).

Since p16^{-/-} macrophages display increased AAM ϕ marker expression after IL-4-induced polarization and since AAM ϕ exert paracrine anti-inflammatory effects²⁹, the functional effects of p16^{INK4a}-deficiency on IL-4-induced macrophage polarization were analyzed by indirect co-culture experiments. Hereto, conditioned medium from IL-4-polarized p16^{-/-} or p16^{+/+} AAM ϕ was added to p16^{+/+} BMDM and their response to LPS was measured (Figure 3G). Conditioned medium from p16^{-/-} AAM ϕ resulted in a more pronounced inhibition of LPS-induced secretion of IL-6 and TNF (Figure 3H, I). Thus, medium from p16^{-/-} AAM ϕ more potently inhibits pro-inflammatory responses.

Collectively, these results evidence that p16^{INK4a}-deficiency results in a phenotype partially resembling IL-4-induced macrophage polarization. Moreover, IL-4-polarized p16^{-/-} macrophages display a more pronounced AAM ϕ phenotype.

p16^{INK4a}-deficient macrophages are more responsive to IL-4, while they respond less to IFN γ or LPS.

Since p16^{-/-} BMDM resemble IL-4-polarized macrophages and since p16^{-/-} AAM ϕ show more potent anti-inflammatory effects than wild type macrophages, the response of p16^{-/-} BMDM to acute (24h) IL-4 activation was assessed. Interestingly, IL-4 treatment resulted in a larger increase of Arg-I, Ym1/2 and Mgl2 mRNA in p16^{-/-} compared to p16^{+/+} BMDM (Figure 4A-C). AAM ϕ are known to be less sensitive to inflammatory stimuli¹⁹. Therefore, the effects of IFN γ and LPS, two pro-inflammatory stimuli, were tested on these cells. Interestingly, p16^{-/-} BMDM

were less responsive to IFN γ , shown by the lower induction of the IFN γ target genes iNOS, Cxcl10 and MHCII (Figure 4D-F), as well as to LPS, shown by the decreased response of the LPS-regulated genes TNF, IL-6 and MCP-1 (Figure 4G-I). Expression levels of the cognate receptors for IL-4, IFN γ and LPS was similar in both genotypes (Figure S4A-C), suggesting that the altered responses were not due to differences in receptor expression.

Collectively, these data show that p16^{-/-} BMDM are more responsive to alternative activation by IL-4 and less responsive to the classical macrophage activators IFN γ and LPS.

Haematopoietic p16^{INK4a}-deficiency increases hepatic expression of alternatively activated macrophage markers upon *S. mansoni* infection.

Since helminth parasite infections induce a strong Th2 immune response resulting in AAM ϕ differentiation^{20, 30}, the influence of p16^{INK4a}-deficiency on macrophage polarization *in vivo* was investigated during *S. mansoni* infection. To assess the role of p16^{INK4a} specifically in haematopoietic cells, p16^{+/+} and p16^{-/-} bone marrow was transplanted in lethally irradiated wild type recipients. Mice were sacrificed 9 weeks after infection, corresponding to the peak of the Th2 immune response, and the hepatic pathology was subsequently characterized.

Expression of Th2 and Th1 cytokines in livers (Figure S5A-D) and spleens (Figure S6A-C), hepatic infection parameters (Table 1), plasma IgE levels (Figure S7), eosinophil infiltration (Table 1), as well as mortality and weight loss (data not shown) did not differ between p16^{-/-} and p16^{+/+} transplanted animals. These results indicate that there are no differences in the lymphocyte-dependent Th2 response, in line with the very low expression of p16^{INK4a} in T-cells (Figure 1A).

Since macrophages express significant levels of p16^{INK4a} (Figure 1A) and since these cells are abundant in *S. mansoni*-induced granulomas²⁰, macrophage markers were measured in the livers of infected mice. Hepatic mRNA levels of F4/80, CD68 and CD14 were equally induced upon infection (Figure 5A-C), indicating that macrophage numbers were not modified. However, the induction of the AAM ϕ markers Ym1/2 (Figure 5D), Fizz1 (Figure 5E)

and Mgl2 (Figure 5F) was higher in mice transplanted with p16^{-/-} vs. p16^{+/+} bone marrow. Moreover, expression of the tissue remodeling markers α SMA and Timp1 (Fig. S5E, F) was higher in mice transplanted with p16^{-/-} bone marrow, consistent with the tissue remodeling function of AAM ϕ ³¹.

Immunohistochemical analysis showed that the parasite-induced granulomas are highly macrophage-enriched (Figure S8). Moreover, Arg-1, Fizz1 and Ym1 co-localized with the general macrophage marker Moma-2. Surprisingly, the macrophage population within the granulomas appeared heterogeneous, since these markers did not entirely co-localize (Figure S8). Nevertheless, these data suggest that the increase in hepatic AAM ϕ marker expression occurs mainly in macrophages. To unequivocally demonstrate this, the macrophage-positive areas of the granulomas were isolated by laser-capture microdissection from p16^{-/-} and p16^{+/+} bone marrow transplanted mice and mRNA levels were measured. p16^{-/-} granulomas displayed increased Mgl2 and Fizz1 mRNA levels, whereas Ym1/2 mRNA tended to be increased (Figure 5G-I). F4/80, CD68 and CD14 expression were identical, indicating that macrophage numbers did not differ between genotypes (data not shown).

Since macrophage polarization influences T-cell activation^{20, 32}, the *ex vivo* response of splenocytes from mice transplanted with p16^{+/+} or p16^{-/-} bone marrow to soluble *S. mansoni* egg antigen (SEA) was measured. Antigen-independent stimulation of naïve splenocytes by anti-CD3 showed similar IL-4 production (data not shown) suggesting an equal ability of T-cells to synthesize Th2 cytokines, regardless of macrophages within the splenocyte preparation. By contrast, antigen-dependent restimulation with SEA showed a lower production of both IL-4 and IFN γ in splenocytes from p16^{-/-} transplanted mice (Figure S6D, E), while IL-10 production was similar (Figure S6F), hence resulting in an unchanged IL-4/IFN γ balance³³.

Collectively, these results provide evidence for a role of p16^{INK4a} in AAM ϕ skewing *in vivo*.

p16^{INK4}-deficiency in macrophages decreases STAT1 and IKK α,β signaling without altering STAT6 phosphorylation.

To unravel the mechanisms underlying the phenotype induced by p16^{INK4a}-deficiency, the microarray data were analyzed to identify which pathways are affected. Interestingly, many genes with a decreased expression in p16^{-/-} BMDM respond to activation of the IFN γ and NF- κ B inflammatory signaling pathways (Figure S9), of which STAT1 and IKK α,β respectively are crucial components. Detailed examination of these gene expression patterns revealed that expression levels were comparable (Cxcl10, ifi27, ifi203, ifi47, ifit1, Ccl5, Irak3, Birc3 and Ly6e) or even lower (ifi44, CD55 and NF κ Bia) in p16^{-/-} BMDM under basal conditions compared to IL-4-polarized p16^{+/+} AAM ϕ (Figure 6). Moreover, most inflammatory genes were more strongly inhibited in IL-4-induced p16^{-/-} AAM ϕ than in p16^{+/+} AAM ϕ (Figure 6 and Figure 2D), suggesting an additive effect of p16^{INK4a}-deficiency on IL-4 treatment. By contrast, such a synergism could not be observed with respect to the AAM ϕ marker genes since many of these AAM ϕ marker genes responded similarly in IL-4-induced p16^{-/-} and p16^{+/+} AAM ϕ (Table S4 and Figure 2D). Collectively, these data show that the pathways controlling IFN γ , NF- κ B, and IL-4 signaling are affected by p16^{INK4a}-deficiency in macrophages.

To determine whether the observed differences were related to indirect effects through pRb, BMDM were treated with CINK4, a potent inhibitor of pRb hyperphosphorylation³⁴. CINK4 treatment resulted in a dose-dependent decrease of cyclin D mRNA levels both in p16^{+/+} and p16^{-/-} BMDM (Figure S3). Furthermore, treatment with CINK4 in combination with IFN γ did not influence the different phenotype between the two genotypes (Figure S10), thus excluding a role for pRb therein.

STAT6 is the major transcription factor activated by IL-4. Surprisingly, IL-4 treatment induced STAT6 phosphorylation to a similar extent in p16^{-/-} and p16^{+/+} BMDM (Figure 7A). By contrast, IFN γ -induced STAT1 phosphorylation (Figure 7B) and LPS-induced IKK α,β phosphorylation were markedly diminished (Figure 7C) in p16^{-/-} vs. p16^{+/+} BMDM.

Interestingly, I κ B α protein levels were increased in p16^{-/-} BMDM under basal conditions (Figure 7C). However, phosphorylation of p38, another downstream target of TLR-4, was not different between p16^{-/-} and p16^{+/+} BMDM (Figure 7C), suggesting that p16^{INK4a}-deficiency specifically alters the NF- κ B response.

Several genes coding for proteins with acetyl transferase activity were induced in p16^{-/-} BMDM (Table 2). Acetylation of STAT1 and IKK α,β inhibits their phosphorylation and thereby their transcriptional activity^{35, 36}. Immunoprecipitation of acetylated proteins revealed that STAT1 and IKK α,β were acetylated to a higher extent in p16^{-/-} than in p16^{+/+} BMDM (Figure 7D). To identify whether STAT1 acetylation is the cause or the consequence of decreased STAT1 phosphorylation, JAK2 phosphorylation, which is upstream in this pathway, was assessed. JAK2 phosphorylation was less pronounced under basal conditions and after activation with IFN γ in p16^{-/-} BMDM (Figure 7E). Since acetylation of STAT1 can interfere with NF- κ B signaling³⁶ and both pathways act synergistically³⁷, the decreased STAT1 and NF- κ B signaling and their increased acetylation probably results from decreased JAK2 phosphorylation.

DISCUSSION

We identify a novel role for the tumor suppressor protein p16^{INK4a} in the regulation of the macrophage phenotype *in vitro* and *in vivo*. p16^{INK4a}-deficiency promotes a STAT6-independent IL4-induced macrophage polarization, whereas LPS and IFN γ responses are lower. These actions of p16^{INK4a}-deficiency likely occur through modification of the JAK2-STAT1 and NF- κ B pathways,

Although p16^{INK4a} is mainly known as a cell cycle inhibitor, cell cycle and macrophage maturation were unaffected in the absence of p16^{INK4a}, and an E2F target gene signature³⁸,³⁹, which would be expected to be increased by p16^{INK4a}-deficiency, could not be identified in p16^{-/-} BMDM. Since p15^{INK4b} is a critical tumor suppressor in the absence of p16^{INK4a}⁴⁰ and since an increase of p15^{INK4b} expression was observed in p16^{-/-} BMDM, a compensatory mechanism between these CDKI might have taken place with respect to cell cycle control.

Interestingly, p16^{INK4a} has been previously shown to modulate transcriptional activities of the pro-inflammatory transcription factors NF- κ B and AP-1. Via its ankyrin motifs, p16^{INK4a} binds c-jun⁴¹ and NF- κ B⁴², inhibiting their activity in several immortalized cell lines. However, this mechanism does not appear to play a role in primary murine macrophages, where the loss of p16^{INK4a} has anti-inflammatory effects. Another CDKI, p21^{WAF1/CIP1}, was also reported to modulate inflammation without altering cell cycle or differentiation. However, in contrast with p16^{INK4a}-deficiency, p21^{WAF1/CIP1}-deficiency in macrophages resulted in a higher sensitivity to inflammatory stimuli^{43, 44}. Additionally, p21^{WAF1/CIP1} expression was unchanged in p16^{-/-} BMDM.

In a model of AAM ϕ differentiation *in vivo*, infection with the helminth *S. mansoni* resulted in equal Th2-associated responses in p16^{-/-} and p16^{+/+} bone marrow transplanted mice. These observations indicate unaltered T-lymphocyte function, in line with the low expression levels of p16^{INK4a} in these cells. By contrast, AAM ϕ markers were significantly increased in the livers and in hepatic granulomas of p16^{-/-} bone marrow transplanted animals, probably due to a cell-autonomous activity of p16^{INK4a} in macrophages. Since total bone marrow was

transplanted, a contribution of other haematopoietic cell types to this cell-autonomous macrophage response cannot be excluded. However, since expression of the measured markers was also up-regulated in the macrophage-rich granulomas and since AAM ϕ markers co-localized with macrophages in the granuloma, the effects are, at least in part, due to p16^{INK4a}-deficiency in the macrophages. Surprisingly, different AAM ϕ markers did not strictly co-localize, suggesting the existence of different macrophage populations in defined regions of the granuloma, which could be due to different gradients of stimuli within the granuloma.

Microarray analysis showed that p16^{-/-} BMDM under basal conditions display a gene signature resembling that of IL-4-induced macrophage polarization ²⁷, with the exception of the AAM ϕ marker genes Ym1/2 and Fizz1. Moreover, p16^{-/-} BMDM were more responsive to IL-4 activation and displayed weaker pro-inflammatory responses to IFN γ and LPS. Importantly, our data show that p16^{INK4a}-deficiency does not influence pRb-mediated activation of the E2F transcription factor. The decreased IFN γ -induced phosphorylation of STAT1 and the LPS-induced IKK α,β phosphorylation in p16^{-/-} BMDM probably account for the attenuated inflammatory responses. Decreased IKK α,β phosphorylation combined with increased I κ B α protein levels correlated with the profound decrease of NF- κ B target gene expression in p16^{-/-} BMDM. Since a cluster of genes coding for proteins with acetyl transferase activity was induced in p16^{-/-} BMDM and since STAT1 ³⁶ and IKK α,β ³⁵ acetylation reduces their ability to be phosphorylated, the decrease in STAT1 and IKK α,β phosphorylation may result from increased acetylation of these proteins in p16^{-/-} BMDM. The acetylation-phosphorylation balance may be influenced by alterations upstream in the signaling pathway. Since phosphorylation of JAK2, the first component to be phosphorylated upon receptor dimerization ⁴⁵, was decreased, it appears that the p16^{INK4a}-deficiency-induced defect in JAK2 phosphorylation may be implicated in the reduced Stat1 phosphorylation. The increased acetylation status may be a consequence of this mechanism, contributing to the phenotype of p16^{-/-} BMDM. Moreover, JAK2 phosphorylation was less pronounced already under basal culture conditions, in line with the observation that p16^{INK4a}-deficiency confers a

lower basal inflammatory phenotype, which is further exacerbated upon stimulation. Since p16^{INK4a}-deficiency alters the IFN γ response early in the pathway and TLR4 signaling only at the level of NF- κ B, but not, for example, at the level of p38, p16^{INK4a}-deficiency thus likely acts directly on the IFN γ and indirectly on the NF- κ B signaling pathway.

Surprisingly, STAT6 phosphorylation, the major transcription factor for IL-4-mediated signaling response, was comparable in BMDM of both genotypes, although IL-4-responsive genes were increased in p16^{-/-} BMDM, suggesting that other pathways are involved. It has been shown that STAT1 activation antagonizes expression of STAT6-induced AAM ϕ marker genes^{46, 47} and that decreased STAT1 phosphorylation can result in an increase of AAM ϕ marker genes⁴⁸ by a number of molecular mechanisms. First, IL-4 action is inhibited by STAT1 activation through inhibition of STAT6 phosphorylation and its subsequent nuclear translocation in human monocytes⁴⁹. However, p16^{INK4a}-deficiency did not modify STAT6 phosphorylation. Second, IFN γ inhibits STAT6 activation by inducing the expression of the suppressor of cytokine signaling 1 (SOCS1) in macrophages⁴⁶. Although SOCS1 mRNA levels were not different between p16^{-/-} and p16^{+/+} BMDM (data not shown), we cannot exclude its involvement via post-transcriptional mechanisms. Third, STAT1 and STAT6 have been shown to compete for binding the same promoters⁴⁷, since decreased STAT1 activity increases binding of STAT6 to the promoters of several of its target genes. To our knowledge, an effect of NF- κ B signaling on STAT6-dependent gene expression has not yet been demonstrated. Therefore, it is possible that the AAM ϕ -like phenotype of p16^{-/-} BMDM is secondary to the decreased CAM ϕ -associated response via JAK2-STAT1.

In conclusion, our results identify p16^{INK4a} as a novel modulator of macrophage polarization and show that p16^{INK4a}-deficiency skews macrophages towards an IL-4-like phenotype. Since the *CDKN2A* locus is predictive for the risk of T2D and CVD^{14, 15}, in which macrophage polarization plays a role^{28, 50}, the role of p16^{INK4a} in the control of macrophage function could be one mechanism contributing to the association of this locus with these diseases.

ACKNOWLEDGMENTS

P.Krimpenfort provided p16^{INK4a}-deficient mice. Discussions with G.Raes, J.Vanginderachter and M.de Winther are greatly acknowledged. We thank E.Vallez for mouse breeding, J.Brozek (Genfit SA, Loos, France) for microarray raw data analysis, T.Coevoet, N.Jouy and A.Lucas for technical assistance. This work was supported by the Fondation pour la Recherche Médicale (DCV20070409276 to B.S.), the EFSD/GSK Program 2009, the Cost Action (BM0602) and the Conseil régional Nord Pas-de-Calais and FEDER. C.Cudejko was supported by a doctoral fellowship from the Nouvelle Société Française d'Athérosclérose/Schering-Plough/MSD. K.Wouters was supported by a European FP7 Marie Curie grant (PIEF-GA-2009-235221) and a European Atherosclerosis Society grant. The funders had no role in study design, data collection and analysis, decision to publish, or preparation of the manuscript.

AUTHORSHIP

C.C. and K.W. designed and performed experiments, analyzed data and wrote the manuscript. L.F., S.A.H., C.P., K.B., E.B., J.V., S.F. and P.R. contributed to some of the experiments. A.T. and G.C contributed to interpret data. D.D., B.S., R.P. contributed to interpretation of the data, manuscript preparation and project supervision. The authors declare no competing financial interests.

ABBREVIATIONS

AAM ϕ	Alternatively activated macrophage
BMDM	Bone marrow-derived macrophages
CAM ϕ	Classically activated macrophage
CDK	Cyclin-dependent kinase
CDKI	Cyclin-dependent kinase inhibitor
DC	Dendritic cell
IFN γ	Interferon gamma
IL	Interleukin
LPS	Lipopolysaccharide
p16 ^{-/-}	p16 ^{INK4a} -deficient
p16 ^{+/+}	Wild type
QPCR	Quantitative polymerase chain reaction
SEA	Soluble egg antigen
SOCS1	Suppressor of cytokine signaling 1
STAT	Signal transducer and activator of transcription
T2D	Type 2 diabetes

References

- [1] Serrano M, Hannon GJ, and Beach D. A new regulatory motif in cell-cycle control causing specific inhibition of cyclin D/CDK4. *Nature* 1993; 366: 704-7.
- [2] Hannon GJ, and Beach D. p15INK4B is a potential effector of TGF-beta-induced cell cycle arrest. *Nature* 1994; 371: 257-61.
- [3] Guan KL, Jenkins CW, Li Y, Nichols MA, Wu X, O'Keefe CL, Matera AG, and Xiong Y. Growth suppression by p18, a p16INK4/MTS1- and p14INK4B/MTS2-related CDK6 inhibitor, correlates with wild-type pRb function. *Genes Dev.* 1994; 8: 2939-52.
- [4] Chan FK, Zhang J, Cheng L, Shapiro DN, and Winoto A. Identification of human and mouse p19, a novel CDK4 and CDK6 inhibitor with homology to p16ink4. *Mol. Cell. Biol.* 1995; 15: 2682-8.
- [5] Hirai H, Roussel MF, Kato JY, Ashmun RA, and Sherr CJ. Novel INK4 proteins, p19 and p18, are specific inhibitors of the cyclin D-dependent kinases CDK4 and CDK6. *Mol. Cell. Biol.* 1995; 15: 2672-81.
- [6] Sharpless NE. INK4a/ARF: a multifunctional tumor suppressor locus. *Mutat. Res.* 2005; 576: 22-38.
- [7] Alcorta DA, Xiong Y, Phelps D, Hannon G, Beach D, and Barrett JC. Involvement of the cyclin-dependent kinase inhibitor p16 (INK4a) in replicative senescence of normal human fibroblasts. *Proc. Natl. Acad. Sci. U.S.A.* 1996; 93: 13742-7.
- [8] Hara E, Smith R, Parry D, Tahara H, Stone S, and Peters G. Regulation of p16CDKN2 expression and its implications for cell immortalization and senescence. *Mol. Cell. Biol.* 1996; 16: 859-67.
- [9] Krishnamurthy J, Torrice C, Ramsey MR, Kovalev GI, Al-Regaiey K, Su L, and Sharpless NE. Ink4a/Arf expression is a biomarker of aging. *J. Clin. Invest.* 2004; 114: 1299-307.
- [10] Nielsen GP, Stemmer-Rachamimov AO, Shaw J, Roy JE, Koh J, and Louis DN. Immunohistochemical survey of p16INK4A expression in normal human adult and infant tissues. *Lab. Invest.* 1999; 79: 1137-43.

- [11] Zindy F, Quelle DE, Roussel MF, and Sherr CJ. Expression of the p16INK4a tumor suppressor versus other INK4 family members during mouse development and aging. *Oncogene* 1997; 15: 203-11.
- [12] Melzer D, Frayling TM, Murray A, Hurst AJ, Harries LW, Song H, Khaw K, Luben R, Surtees PG, Bandinelli SS, Corsi A, Ferrucci L, Guralnik JM, Wallace RB, Hattersley AT, and Pharoah PD. A common variant of the p16(INK4a) genetic region is associated with physical function in older people. *Mech. Ageing Dev.* 2007; 128: 370-7.
- [13] Janzen V, Forkert R, Fleming HE, Saito Y, Waring MT, Dombkowski DM, Cheng T, DePinho RA, Sharpless NE, and Scadden DT. Stem-cell ageing modified by the cyclin-dependent kinase inhibitor p16INK4a. *Nature* 2006; 443: 421-6.
- [14] McPherson R, Pertsemlidis A, Kavaslar N, Stewart A, Roberts R, Cox DR, Hinds DA, Pennacchio LA, Tybjaerg-Hansen A, Folsom AR, Boerwinkle E, Hobbs HH, and Cohen JC. A common allele on chromosome 9 associated with coronary heart disease. *Science* 2007; 316: 1488-91.
- [15] Liu Y, Sanoff HK, Cho H, Burd CE, Torrice C, Mohlke KL, Ibrahim JG, Thomas NE, and Sharpless NE. INK4/ARF transcript expression is associated with chromosome 9p21 variants linked to atherosclerosis. *PLoS One* 2009; 4: e5027.
- [16] Saxena R, Voight BF, Lyssenko V, Burt NP, de Bakker PIW, Chen H, Roix JJ, Kathiresan S, Hirschhorn JN, Daly MJ, Hughes TE, Groop L, Altshuler D, Almgren P, Florez JC, Meyer J, Ardlie K, Bengtsson Boström K, Isomaa B, Lettre G, Lindblad U, Lyon HN, Melander O, Newton-Cheh C, Nilsson P, Orho-Melander M, Råstam L, Speliotes EK, Taskinen M, Tuomi T, Guiducci C, Berglund A, Carlson J, Gianniny L, Hackett R, Hall L, Holmkvist J, Laurila E, Sjögren M, Sterner M, Surti A, Svensson M, Svensson M, Tewhey R, Blumenstiel B, Parkin M, Defelice M, Barry R, Brodeur W, Camarata J, Chia N, Fava M, Gibbons J, Handsaker B, Healy C, Nguyen K, Gates C, Sougnez C, Gage D, Nizzari M, Gabriel SB, Chirn G, Ma Q, Parikh H, Richardson D, Ricke D, and Purcell S. Genome-wide association analysis identifies loci for type 2 diabetes and triglyceride levels. *Science* 2007; 316: 1331-6.

- [17] Wei S, Lightwood D, Ladyman H, Cross S, Neale H, Griffiths M, Adams R, Marshall D, Lawson A, McKnight AJ, and Stanley ER. Modulation of CSF-1-regulated post-natal development with anti-CSF-1 antibody. *Immunobiology* 2005; 210: 109-19.
- [18] Baffy G. Kupffer cells in non-alcoholic fatty liver disease: the emerging view. *J. Hepatol.* 2009; 51: 212-23.
- [19] Gordon S. Alternative activation of macrophages. *Nat. Rev. Immunol.* 2003; 3: 23-35.
- [20] Herbert DR, Hölscher C, Mohrs M, Arendse B, Schwegmann A, Radwanska M, Leeto M, Kirsch R, Hall P, Mossmann H, Claussen B, Förster I, and Brombacher F. Alternative macrophage activation is essential for survival during schistosomiasis and downmodulates T helper 1 responses and immunopathology. *Immunity* 2004; 20: 623-35.
- [21] Bellocchia S, Via D, Canavesi M, Pfister P, Fumagalli R, Paoletti R, and Bernini F. HMG-CoA reductase inhibitors reduce MMP-9 secretion by macrophages. *Arterioscler. Thromb. Vasc. Biol.* 1998; 18: 1671-8.
- [22] Dubois A, Deruytter N, Adams B, Kanda A, Delbauve S, Fleury S, Torres D, François A, Péteïn M, Goldman M, Dombrowicz D, and Flamand V. Regulation of Th2 Responses and Allergic Inflammation through Bystander Activation of CD8+ T Lymphocytes in Early Life. *J. Immunol.* 2010; : .
- [23] Van Ginderachter JA, Movahedi K, Hassanzadeh Ghassabeh G, Meerschaut S, Beschin A, Raes G, and De Baetselier P. Classical and alternative activation of mononuclear phagocytes: picking the best of both worlds for tumor promotion. *Immunobiology* 2006; 211: 487-501.
- [24] Vats D, Mukundan L, Odegaard JI, Zhang L, Smith KL, Morel CR, Wagner RA, Greaves DR, Murray PJ, and Chawla A. Oxidative metabolism and PGC-1beta attenuate macrophage-mediated inflammation. *Cell Metab* 2006; 4: 13-24.
- [25] Martinez FO, Gordon S, Locati M, and Mantovani A. Transcriptional profiling of the human monocyte-to-macrophage differentiation and polarization: new molecules and patterns of gene expression. *J. Immunol.* 2006; 177: 7303-11.

- [26] Noël W, Raes G, Hassanzadeh Ghassabeh G, De Baetselier P, and Beschin A. Alternatively activated macrophages during parasite infections. *Trends Parasitol.* 2004; 20: 126-33.
- [27] Mantovani A, Sica A, Sozzani S, Allavena P, Vecchi A, and Locati M. The chemokine system in diverse forms of macrophage activation and polarization. *Trends Immunol.* 2004; 25: 677-86.
- [28] Bouhlel MA, Derudas B, Rigamonti E, Dièvert R, Brozek J, Haulon S, Zawadzki C, Jude B, Torpier G, Marx N, Staels B, and Chinetti-Gbaguidi G. PPAR γ activation primes human monocytes into alternative M2 macrophages with anti-inflammatory properties. *Cell Metab* 2007; 6: 137-43.
- [29] Katakura T, Miyazaki M, Kobayashi M, Herndon DN, and Suzuki F. CCL17 and IL-10 as effectors that enable alternatively activated macrophages to inhibit the generation of classically activated macrophages. *J. Immunol.* 2004; 172: 1407-13.
- [30] Pearce EJ, Kane C, Sun J, Taylor J, McKee AS, and Cervi L. Th2 response polarization during infection with the helminth parasite *Schistosoma mansoni*. *Immunol. Rev.* 2004; 201: 117-26.
- [31] Wynn TA. Fibrotic disease and the T(H)1/T(H)2 paradigm. *Nat. Rev. Immunol.* 2004; 4: 583-94.
- [32] Elliott DE, and Boros DL. Schistosome egg antigen(s) presentation and regulatory activity by macrophages isolated from vigorous or immunomodulated liver granulomas of *Schistosoma mansoni*-infected mice. *J. Immunol.* 1984; 132: 1506-10.
- [33] Mosmann TR, and Coffman RL. TH1 and TH2 cells: different patterns of lymphokine secretion lead to different functional properties. *Annu. Rev. Immunol.* 1989; 7: 145-73.
- [34] Soni R, O'Reilly T, Furet P, Muller L, Stephan C, Zumstein-Mecker S, Fretz H, Fabbro D, and Chaudhuri B. Selective in vivo and in vitro effects of a small molecule inhibitor of cyclin-dependent kinase 4. *J. Natl. Cancer Inst.* 2001; 93: 436-46.

- [35] Mittal R, Peak-Chew S, and McMahon HT. Acetylation of MEK2 and I kappa B kinase (IKK) activation loop residues by YopJ inhibits signaling. *Proc. Natl. Acad. Sci. U.S.A.* 2006; 103: 18574-9.
- [36] Krämer OH, Baus D, Knauer SK, Stein S, Jäger E, Stauber RH, Grez M, Pfitzner E, and Heinzl T. Acetylation of Stat1 modulates NF-kappaB activity. *Genes Dev.* 2006; 20: 473-85.
- [37] Hiroi M, and Ohmori Y. The transcriptional coactivator CREB-binding protein cooperates with STAT1 and NF-kappa B for synergistic transcriptional activation of the CXC ligand 9/monokine induced by interferon-gamma gene. *J. Biol. Chem.* 2003; 278: 651-60.
- [38] Vernell R, Helin K, and Müller H. Identification of target genes of the p16INK4A-pRB-E2F pathway. *J. Biol. Chem.* 2003; 278: 46124-37.
- [39] Stanelle J, Stiewe T, Theseling CC, Peter M, and Pützer BM. Gene expression changes in response to E2F1 activation. *Nucleic Acids Res.* 2002; 30: 1859-67.
- [40] Krimpenfort P, Ijpenberg A, Song J, van der Valk M, Nawijn M, Zevenhoven J, and Berns A. p15Ink4b is a critical tumour suppressor in the absence of p16Ink4a. *Nature* 2007; 448: 943-6.
- [41] Choi BY, Choi HS, Ko K, Cho Y, Zhu F, Kang BS, Ermakova SP, Ma W, Bode AM, and Dong Z. The tumor suppressor p16(INK4a) prevents cell transformation through inhibition of c-Jun phosphorylation and AP-1 activity. *Nat. Struct. Mol. Biol.* 2005; 12: 699-707.
- [42] Wolff B, and Naumann M. INK4 cell cycle inhibitors direct transcriptional inactivation of NF-kappaB. *Oncogene* 1999; 18: 2663-6.
- [43] Scatizzi JC, Mavers M, Hutcheson J, Young B, Shi B, Pope RM, Ruderman EM, Samways DSK, Corbett JA, Egan TM, and Perlman H. The CDK domain of p21 is a suppressor of IL-1beta-mediated inflammation in activated macrophages. *Eur. J. Immunol.* 2009; 39: 820-5.
- [44] Trakala M, Arias CF, García MI, Moreno-Ortiz MC, Tsilingiri K, Fernández PJ, Mellado M, Díaz-Meco MT, Moscat J, Serrano M, Martínez-A C, and Balomenos D.

Regulation of macrophage activation and septic shock susceptibility via p21(WAF1/CIP1).
Eur. J. Immunol. 2009; 39: 810-9.

[45] Shuai K, and Liu B. Regulation of JAK-STAT signalling in the immune system. Nat. Rev. Immunol. 2003; 3: 900-11.

[46] Dickensheets HL, Venkataraman C, Schindler U, and Donnelly RP. Interferons inhibit activation of STAT6 by interleukin 4 in human monocytes by inducing SOCS-1 gene expression. Proc. Natl. Acad. Sci. U.S.A. 1999; 96: 10800-5.

[47] Ohmori Y, and Hamilton TA. IL-4-induced STAT6 suppresses IFN-gamma-stimulated STAT1-dependent transcription in mouse macrophages. J. Immunol. 1997; 159: 5474-82.

[48] Porta C, Rimoldi M, Raes G, Brys L, Ghezzi P, Di Liberto D, Dieli F, Ghisletti S, Natoli G, De Baetselier P, Mantovani A, and Sica A. Tolerance and M2 (alternative) macrophage polarization are related processes orchestrated by p50 nuclear factor kappaB. Proc. Natl. Acad. Sci. U.S.A. 2009; 106: 14978-83.

[49] Dickensheets HL, and Donnelly RP. Inhibition of IL-4-inducible gene expression in human monocytes by type I and type II interferons. J. Leukoc. Biol. 1999; 65: 307-12.

[50] Odegaard JI, Ricardo-Gonzalez RR, Goforth MH, Morel CR, Subramanian V, Mukundan L, Red Eagle A, Vats D, Brombacher F, Ferrante AW, and Chawla A. Macrophage-specific PPARgamma controls alternative activation and improves insulin resistance. Nature 2007; 447: 1116-20.

TABLES

Table 1. Liver pathology during Schistosomiasis

Parameter	p16 ^{-/-} donor	p16 ^{+/+} donor
Male and female worm number	5±1 / 5±1	7±1 / 6±1
Parasite burden (egg number/female/g tissue)	1604±191	1698±359
AST plasma concentration (U/ml)	131±59	115±37
Granuloma number per mm ² liver area	25±2	28±2
Granuloma area / liver area (mm ² /mm ²)	0.078±0.006	0.087±0.009
Eosinophils / granuloma area (mm ²)	12±1	10±1
Collagen area / liver area	0.132±0.023	0.112±0.014

Table 2. Genes coding for proteins with acetyl transferase activity in p16^{INK4a}-deficient macrophages

Probeset	Symbol	Description	fold change	p value
1435224_at	CBP/p300	CREB binding protein	1.96	1,00E-04
1426783_at	Gcn5l2	GCN5 general control of amino acid synthesis-like 2	1.91	2,20E-04
1448711_at	Mcm3ap	minichromosome maintenance deficient 3 associated protein	1.55	8,90E-03
1433692_at	Nat10	N-acetyltransferase 10	1.65	1,80E-04
1419213_at	Nat6	N-acetyltransferase 6	2.11	8,40E-06
1435842_at	Nat8l	N-acetyltransferase 8-like	1.32	4,60E-02
1436580_at	Hgsnat	Heparan-alpha-glucosaminide N-acetyltransferase	1.38	1,80E-02

FIGURE LEGENDS

Figure 1. p16^{INK4a} is expressed, but does not influence maturation or the cell cycle in macrophages.

(A) p16^{INK4a} mRNA expression was measured in immune cells isolated from mice: dendritic cells (DC), bone marrow derived-macrophages (BMDM), neutrophils, B-lymphocytes and T-lymphocytes. (B) p16^{INK4a} mRNA expression was measured at different stages during differentiation of BMDM isolated from p16^{+/+} mice. Since p16^{INK4a} fold induction differs between experiments, data is from one of three distinct experiments. (C) p16^{INK4a} protein expression in p16^{+/+} and p16^{-/-} BMDM was analyzed by Western blot with an anti-p16^{INK4a} antibody. Anti-actin antibody was used as loading control. (D and E) Increase of the macrophage marker F4/80 mRNA expression (D) and protein expression (E) measured by respectively QPCR and flow cytometry in p16^{+/+} and p16^{-/-} BMDM. Data are shown from one of three independent experiments. (F) Cell cycle analysis by propidium iodide staining of p16^{+/+} and p16^{-/-} BMDM during differentiation expressed in % of events \pm standard deviation.

Figure 2. p16^{INK4a}-deficiency induces a gene expression profile resembling IL-4-induced macrophage polarization.

Microarray analysis using mRNA from p16^{-/-} BMDM compared to p16^{+/+} BMDM showed (A) decreased mRNA expression of classically activated macrophages-associated genes and (B) increased mRNA expression of alternatively activated macrophages-associated genes. Data is expressed as fold change relative to p16^{+/+} BMDM. (C) Differential gene expression in p16^{-/-} BMDM relative to p16^{+/+} BMDM was correlated with the changes induced in IL-4-induced p16^{+/+} AAM ϕ . The figure shows 2log values of the probesets significantly ($p < 0.05$) regulated only in p16^{-/-} BMDM (red dots), only in IL-4-polarized p16^{+/+} AAM ϕ (green dots) and by both conditions (blue dots), compared to p16^{+/+} BMDM. The X-axis represents differences in gene expression induced by IL-4, whereas the Y-axis represents the effect of p16^{INK4a}-deficiency. These comparisons are depicted in the schematic representation of the protocol in the corresponding colors. Pearson Correlation analysis was done for probesets

differentially expressed by both conditions (blue). **(D)** Heat map of p16^{+/+} BMDM, p16^{-/-} BMDM, IL-4-polarized p16^{+/+} and p16^{-/-} AAM ϕ gene expression profiles. Colors fluctuate from blue (poorly expressed) to green (intermediate expression) and yellow (high expression). Additional information regarding gene description, fold induction, and p-value can be found in Table S3.

Figure 3. p16^{INK4a}-deficient macrophages phenotypically and functionally resemble IL-4-polarized alternatively activated macrophages.

Protein secretion of IL-6 **(A)**, TNF **(B)**, and IL-1Rn **(C)** was measured in the culture medium of p16^{+/+} and p16^{-/-} BMDM by ELISA. **(D-F)** QPCR analysis of Arg-1 **(D)**, Ym1/2 **(E)**, and Mgl2 **(F)** of p16^{+/+} and p16^{-/-} AAM ϕ polarized by addition of 15 ng/mL IL-4 from day 0 of differentiation. **(G)** Schematic representation of the indirect co-culture experiment. **(H and I)** LPS-induced secretion of IL-6 **(H)**, and TNF **(I)** was determined by ELISA in p16^{+/+} BMDM supernatants resulting from indirect co-culture. Statistically significant differences are indicated (*t*-test; ****p*<0.001 ***p*<0.01, and **p*<0.05).

Figure 4. p16^{INK4a}-deficiency modulates macrophage responses to alternatively and classically polarizing stimuli.

mRNA expression from p16^{+/+} and p16^{-/-} BMDM activated with 15 ng/mL IL-4 during 24h **(A-C)**, 10 ng/mL IFN γ during 12h **(D-F)**, or 100 ng/mL LPS during 2h **(G)** or 24h **(H and I)**. mRNA expression of the IL-4-induced target genes Arg-1 **(A)**, Ym1/2 **(B)**, and Mgl2 **(C)**; IFN γ -induced target genes iNOS **(D)**, Cxcl10 **(E)**, and MHCII **(F)**; and LPS-induced target genes TNF **(G)**, IL-6 **(H)**, and MCP-1 **(I)** was quantified by QPCR and expressed as fold increase compared with respective controls. Statistically significant differences are indicated (*t*-test; ****p*<0.001 ***p*<0.01, and **p*<0.05).

Figure 5. Haematopoietic deficiency of p16^{INK4a} exacerbates hepatic alternative macrophage activation of *S. mansoni*-infected mice.

Hepatic mRNA expression from mice transplanted with either p16^{+/+} or p16^{-/-} bone marrow which were not infected (naive) or infected with *S. mansoni*, 9 weeks post-infection. mRNA expression of the macrophage markers F4/80 (A), CD68 (B), and CD14 (C); AAM ϕ markers Ym1/2 (D), Fizz1 (E), and Mgl2 (F) was quantified by QPCR and expressed as fold increase compared to their respective naive controls. Data was obtained from $n=10$ naive and $n=14$ infected mice per genotype. Hepatic granulomas were isolated by laser-capture microdissection and mRNA expression of the AAM ϕ markers Ym1/2 (G), Fizz1 (H), and Mgl2 (I) was quantified by QPCR. Statistically significant differences are indicated (t -test; ** $p<0.01$ and * $p<0.05$).

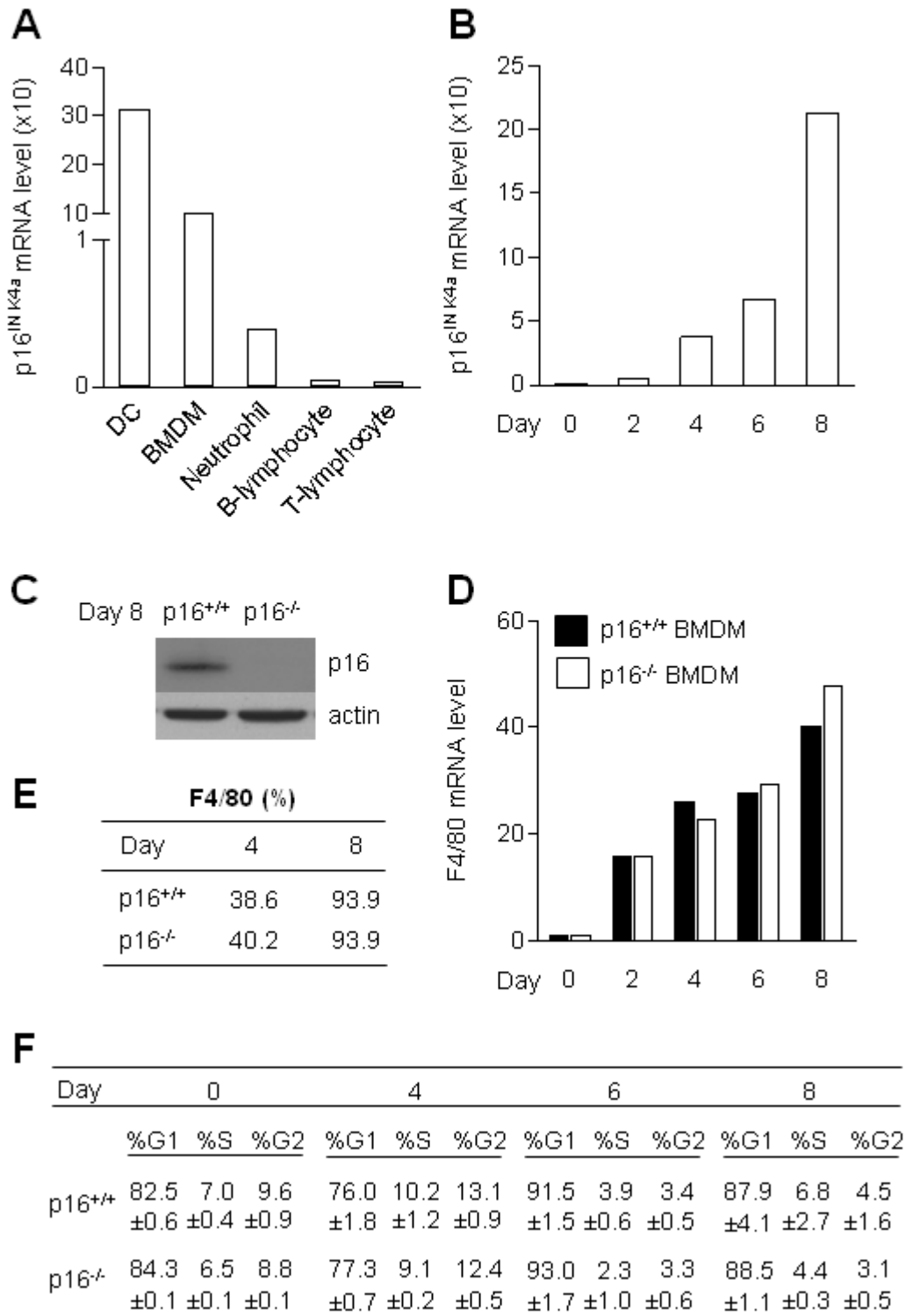
Figure 6. p16^{INK4a}-deficiency results in an alteration of STAT1 and NF- κ B signaling.

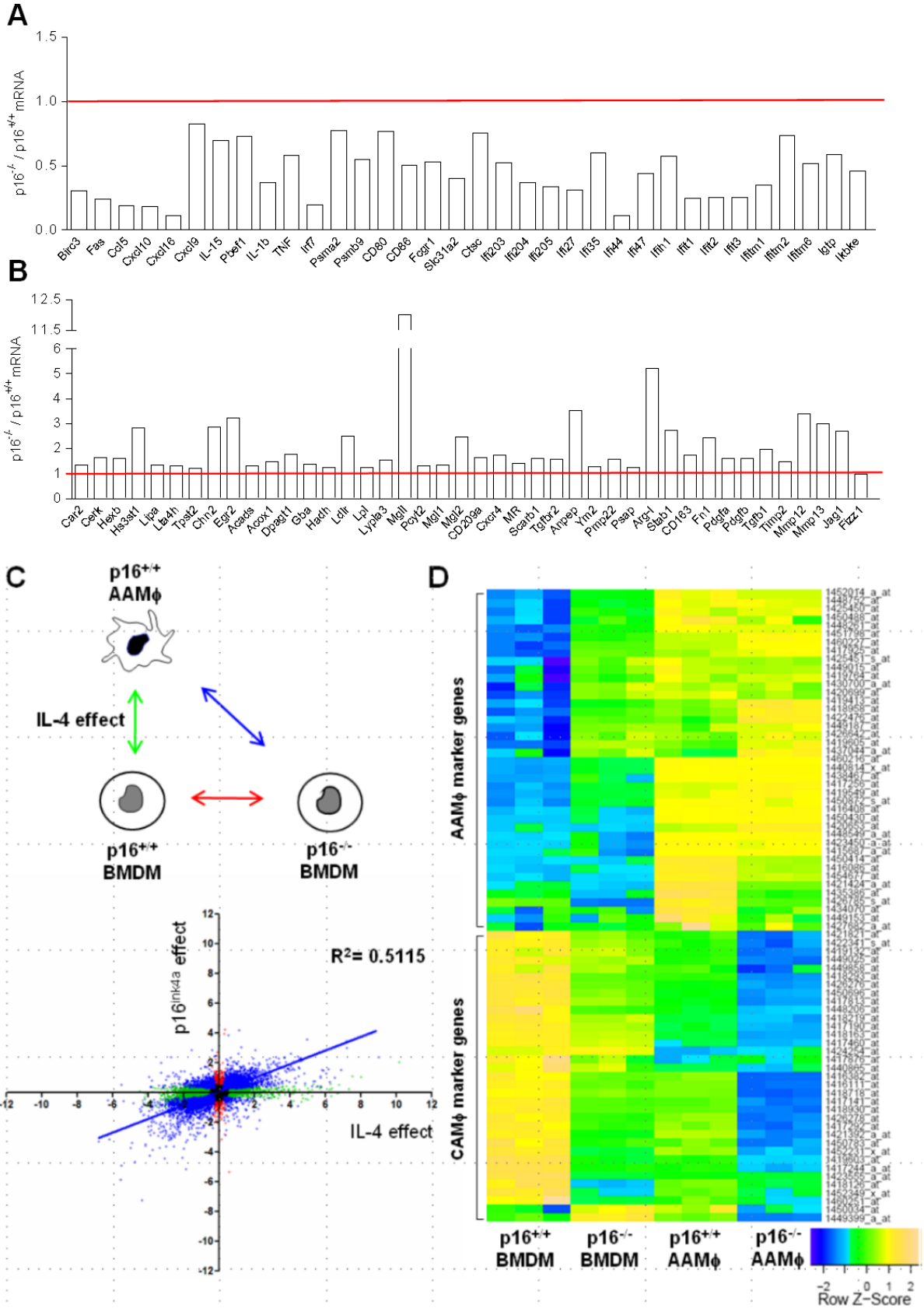
Representation of the relative microarray intensity values from a selection of down-regulated genes in p16^{+/+} and p16^{-/-} BMDM with or without polarization (AAM ϕ) by 15 ng/mL IL-4 from day 0 of differentiation. Statistically significant differences are indicated (a: $p<0.05$ compared to p16^{+/+} BMDM; b: $p<0.05$ compared to p16^{-/-} BMDM; c: $p<0.05$ compared to p16^{+/+} AAM ϕ .)

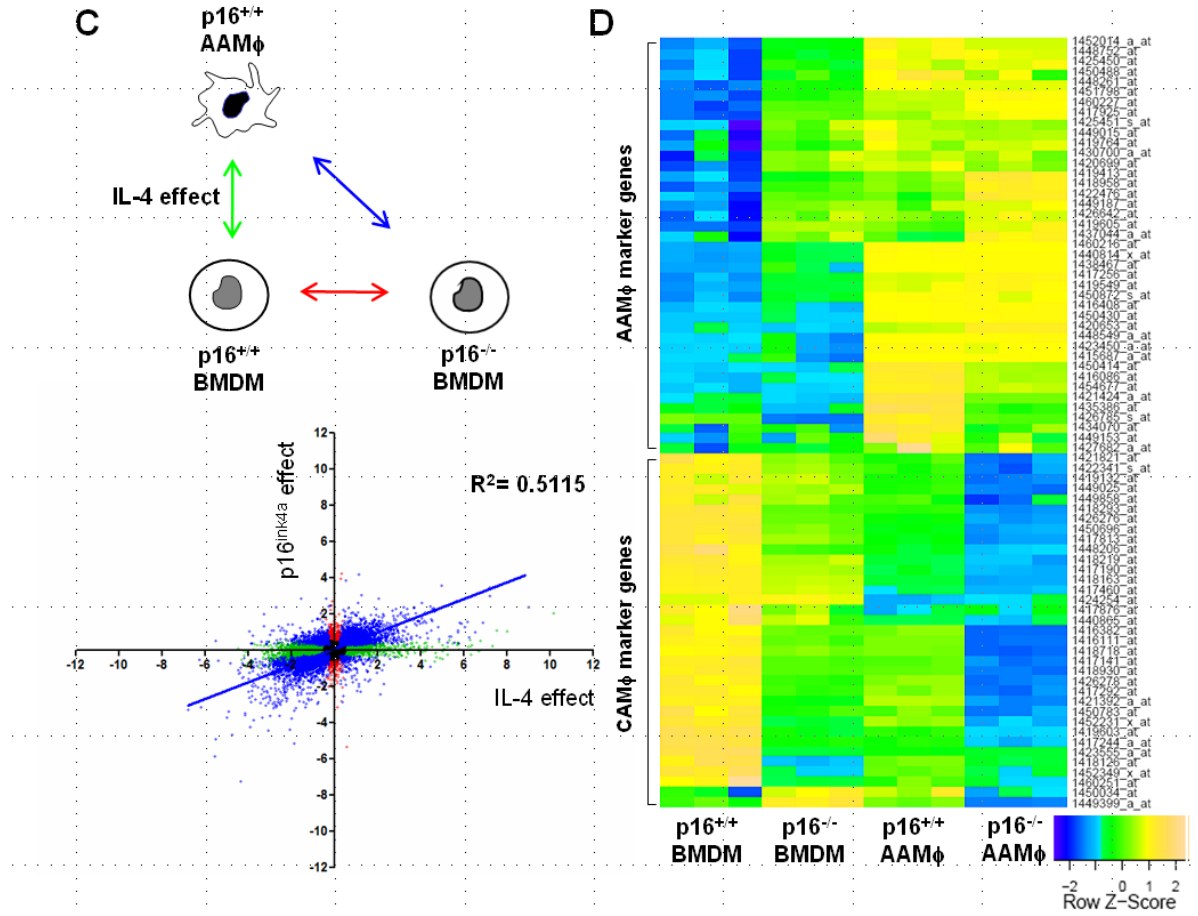
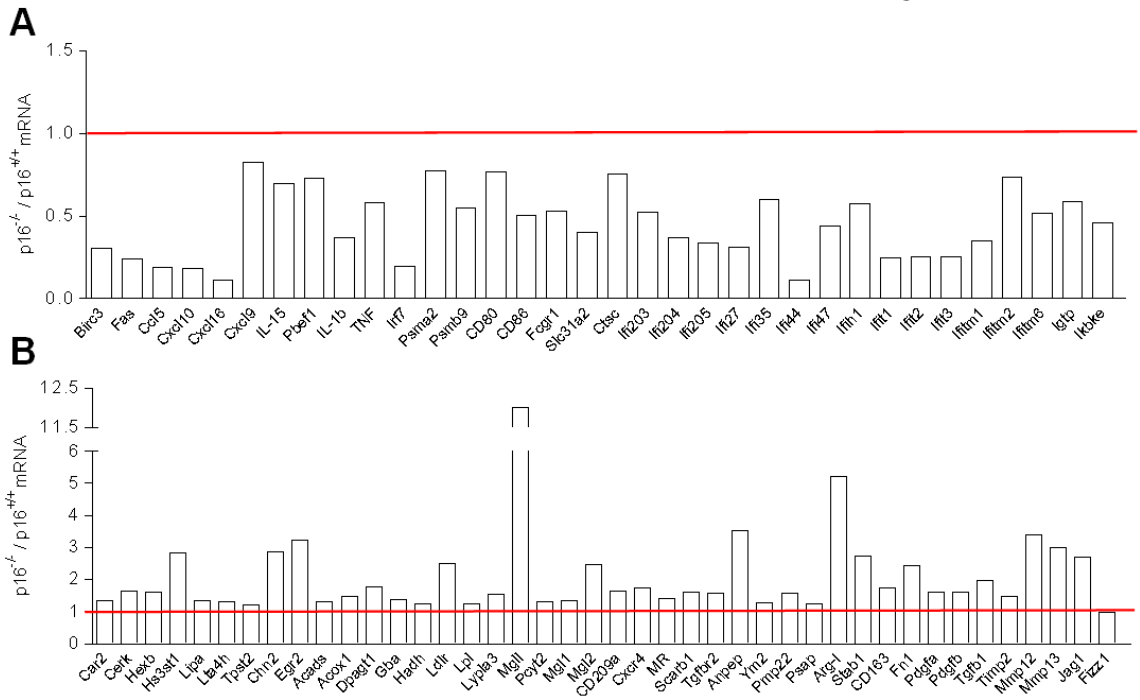
Figure 7. p16^{INK4a}-deficiency diminishes JAK2-STAT1 and NF- κ B signaling and increases acetylation of STAT1 and IKK α,β .

Total protein extracts of p16^{+/+} and p16^{-/-} BMDM treated with 15 ng/mL IL-4 (A), 2.5 ng/mL IFN γ (B) and (E), and 100 ng/mL LPS (C) for the times indicated. Western blots were performed with the indicated antibodies. (D) Total protein extracts from p16^{+/+} and p16^{-/-} BMDM treated with 2.5 ng/mL IFN γ for 5h were then immunoprecipitated (IP) with an anti-Acetyl-Lys antibody and then immunoblotted with an anti-STAT1 antibody or with an anti- $\text{IKK}\alpha,\beta$ antibody, as indicated. Input corresponds to 5% of total protein extract used for IP.

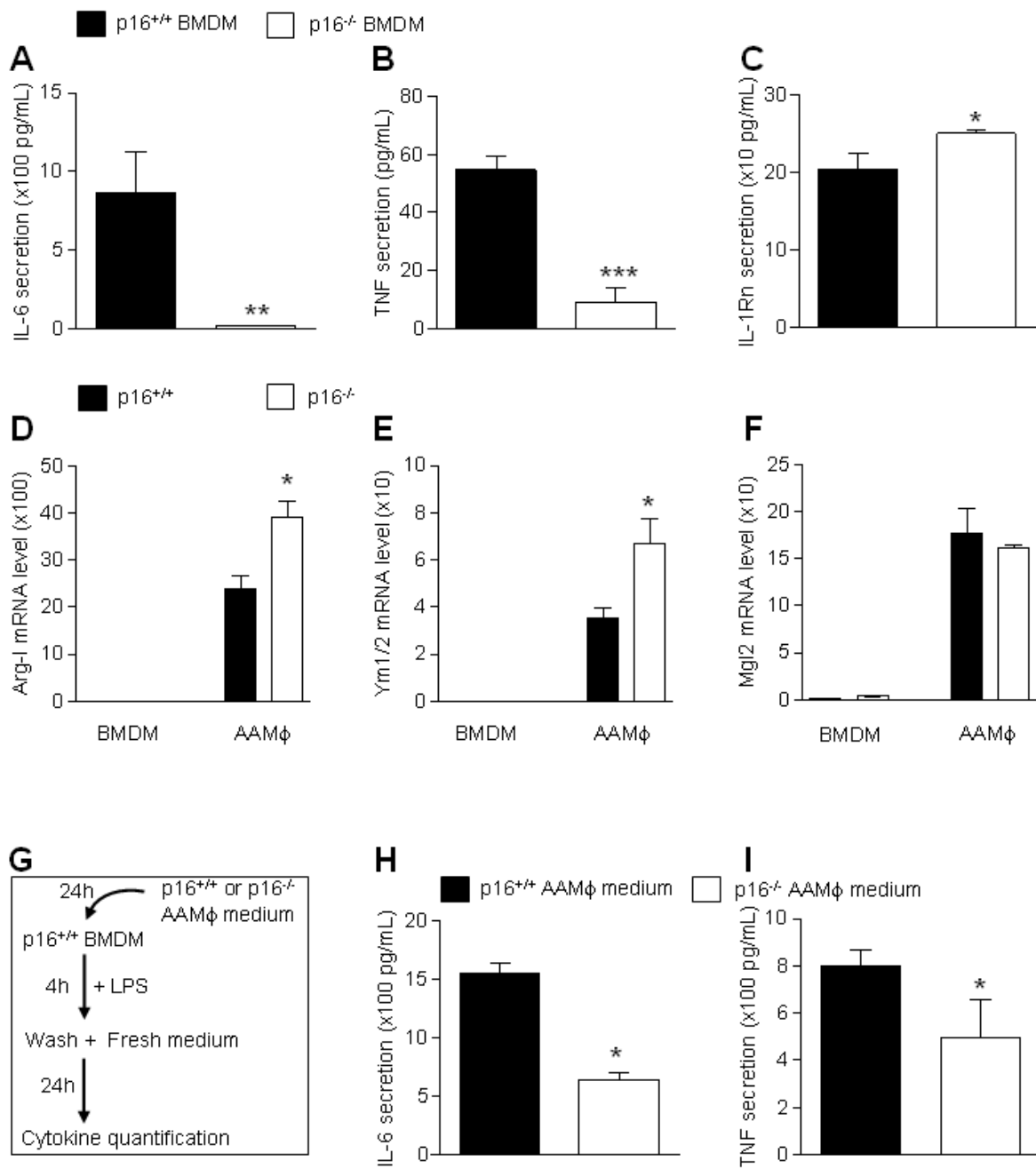
Cudejko-Wouters Fig 1



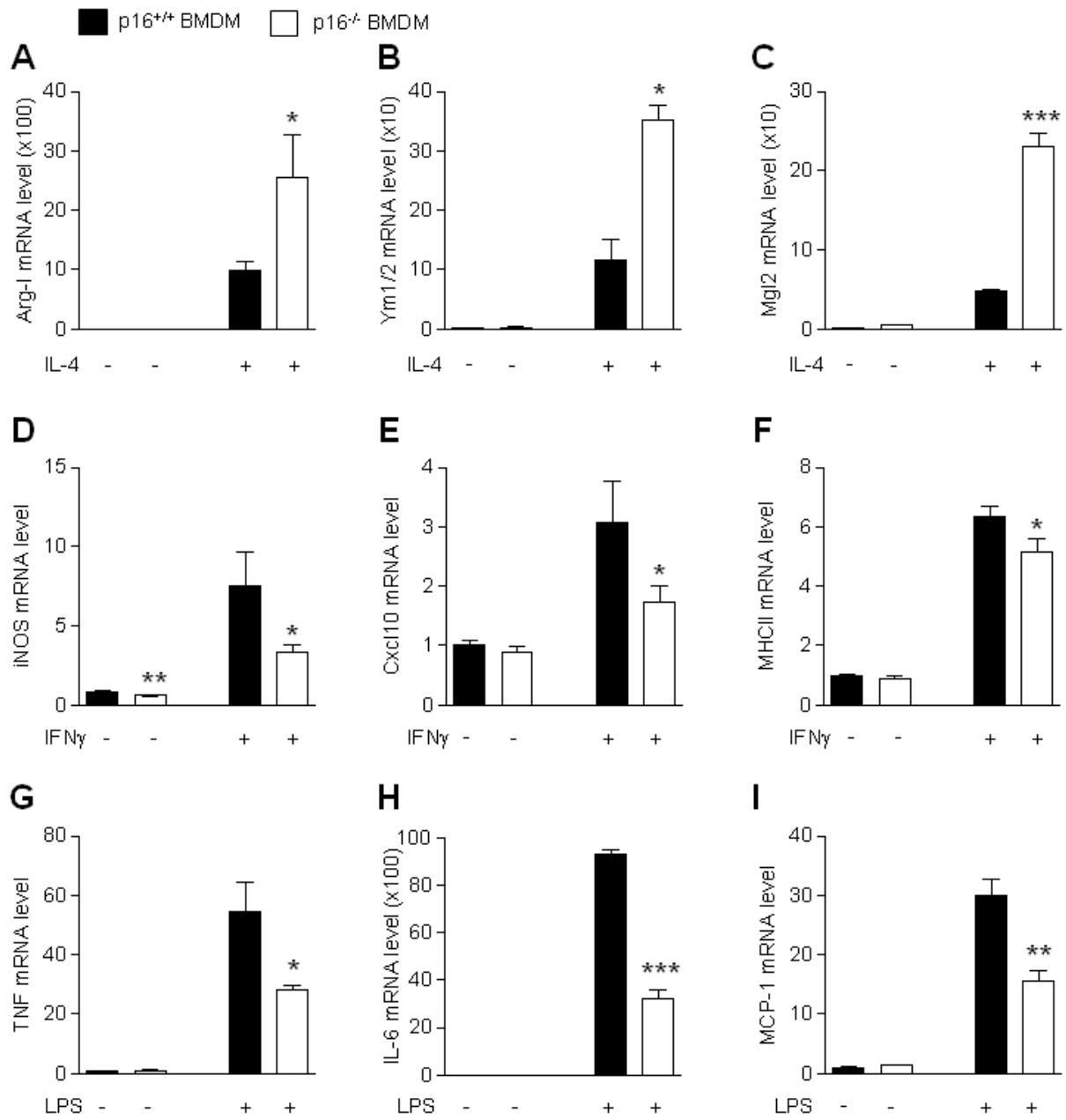




Cudejko-Wouters Fig 3



Cudejko-Wouters Fig 4



Cudejko-Wouters Fig 5

